Residues in *Methylosinus trichosporium* OB3b Methane Monooxygenase Component B Involved in Molecular Interactions with Reduced- and Oxidized-Hydroxylase Component: A Role for the N-Terminus†

Shou-Lin Chang, Bradley J. Wallar, John D. Lipscomb, and Kevin H. Mayo*

Department of Biochemistry, Molecular Biology, and Biophysics and Center for Metals in Biocatalysis, University of Minnesota, 321 Church Street, Minneapolis, Minnesota 55455

Received February 19, 2001; Revised Manuscript Received May 24, 2001

ABSTRACT: Methane monooxygenase (MMO) is a non-heme-iron-containing enzyme which consists of 3 protein components: a hydroxylase (MMOH), an NAD(P)H-linked reductase (MMOR), and a 138-residue regulatory protein, component B (MMOB). Here, NMR spectroscopy has been used to derive interactions between MMOB and reduced and oxidized states of MMOH (245 kDa). Differential broadening of MMOB resonances in ^{1}H-^{15}N HSQC spectra acquired at different molar ratios of MMOH indicates interaction of both proteins, with MMOB binding more tightly to oxidized MMOH as observed previously. The most broadened backbone NH resonances suggest which residues in MMOB are part of the MMOH-binding interface, particularly when those residues are spatially close or clustered in the structure of MMOB. Although a number of different residues in MMOB appear to be involved in interacting with oxidized- and reduced-MMOH, some are identical. The two most common segments, proximal in the structure of MMOB, are β-strand 1 with turn 1 (residues 36−46) and α-helix 3 going into loop 2 (residues 101−112). In addition, the N-terminus of MMOB is observed to be involved in binding to MMOH in either redox state. This is most strongly evidenced by use of a synthetic N-terminal peptide from MMOB (residues 1−29) in differential broadening ^{1}H TOCSY studies with MMOH. Binding specificity is demonstrated by displacement of the peptide from MMOH by parent MMOB, indicating that the peptide binds in or near the normal site of N-terminal binding. The N-terminus is also observed to be functionally important. Steady-state kinetic studies show that neither a Δ2−29 MMOB deletion mutant (which in fact does bind to MMOH), the N-terminal peptide, nor a combination of the two elicit the effector functions of MMOB. Furthermore, transient kinetic studies indicate that none of the intermediates of the MMOH catalytic cycle are observed if either the Δ2−29 MMOB mutant or the N-terminal peptide is used in place of MMOB, suggesting that deletion of the N-terminus prevents reaction of reduced MMOH with O_2 that initiates catalysis.

Methane monooxygenase (MMO)[1] catalyzes the efficient cleavage of the stable C−H bond of methane to yield methanol in an NAD(P)H- and O_2-dependent reaction. The soluble form of the enzyme has been well characterized from both the type II methanotroph *Methylosinus trichosporium* OB3b and the type X methanotroph *Methylococcus capsulatus* (Bath) (*1*−*3*). These enzymes appear to be both structurally and mechanistically similar. The enzyme from *M. trichosporium* OB3b consists of three independent protein components: a 245 kDa hydroxylase component (MMOH) having an $(\alpha\beta\gamma)_2$ subunit structure, a monomeric 38 kDa reductase component (MMOR), and a monomeric 15 kDa regulatory protein termed component B (MMOB) (*1*). MMOR contains FAD and a $[Fe_2S_2]$ cluster that serve to transfer electrons to MMOH from NAD(P)H, while MMOB has no known cofactors. An active site containing a non-heme bis-μ-hydroxo-bridged binuclear iron cluster is found in each of the α subunits of MMOH (*4*−*6*). This diiron cluster has been shown through kinetic and spectroscopic studies to be responsible for O_2 activation and subsequent hydrocarbon oxidation (*7*−*9*). If MMOH is supplied with O_2 and electrons from an artificial donor [or alternatively H_2O_2 as a source of both electrons and oxygen (*10*)], it can catalyze the oxidation of methane without MMOR and MMOB (*1*, *11*). However, both the rate of turnover and the efficiency with which reducing equivalents are coupled to product yield are greatly enhanced by MMOB and, to a lesser extent, MMOR (*1*, *12*, *13*).

† This work was supported by National Institutes of Health Grant R01-GM- 40466 (J.D.L.) and Biophysics Training Grant GM-07323 (B.J.W.).

* To whom correspondence should be addressed at the Department of Biochemistry, Molecular Biology, and Biophysics, University of Minnesota, 6-155 Jackson Hall, 321 Church St., Minneapolis, MN 55455. E-mail: mayox001@maroon.tc.umn.edu. Telephone: (612) 612-625-9968. Fax: (612) 624-5121.

[1] Abbreviations: NMR, nuclear magnetic resonance; rf, radio frequency; FID, free induction decay; CD, circular dichroism; MMO, methane monooxygenase; MMOH, MMO hydroxylase; MMOB, MMO component B; MMOR, MMO reductase; NOE, nuclear Overhauser effect; HSQC, heteronuclear single quantum correlation spectroscopy; HMQC, heteronuclear multiple quantum correlation spectroscopy; COSY, correlation spectroscopy; TOCSY, total correlation spectroscopy; PFG, pulsed field gradient; MOPS, 3-morpholinopropanesulfonic acid; DEAE, diethylaminoethyl; RMSD, root-mean-squared deviation; DSS, 4,4-dimethyl-4-silapentane; T4MOD, toluene monooxygenase component D; P2, phenol hydroxylase component P2.

10.1021/bi0103462 CCC: $20.00
Published on Web 07/19/2001

The effects of MMOB on catalysis are mediated through the formation of a specific complex with the α subunit of MMOH (*14*). As a result of this complex, the rate of multiple turnover is increase up to 150-fold, the rate constant for the reaction with O_2 is increased 1000-fold (*12*), the rate constant of formation of the reactive catalytic cycle intermediate compound Q (**Q**) is increased 40-fold (*12*), the redox potential of the diiron cluster is shifted by −132 mV (*15*), the regiospecificity for oxidation of complex substrates is dramatically altered (*11*), and the spectroscopic features of the diiron cluster are changed, suggesting a conformational change at the active site (*13*−*16*). These effects on catalysis are very dramatic such that essentially no **Q** accumulates in the absence of MMOB, and the time to complete a single turnover at 4 °C is shifted from a few seconds to over 10 min. We have proposed (*12*) that the major role of MMOB is as an O_2-gating protein that allows molecular oxygen to bind and be activated much more efficiently. However, our recent studies have shown that MMOB affects the rate constants of steps throughout the catalytic cycle (*17*).

Although it is clear that structural changes occurring in the MMOH−MMOB complex must be responsible for the regulatory effects described above, neither the specific nature of the interaction nor the structural changes are known in detail. Recently, the X-ray crystal structure of MMOH (*5, 6, 18*) and the NMR solution structure of MMOB (*19, 20*) have been determined for MMO components isolated from both *M. trichosporium* OB3b and *Me. capsulatus* (Bath). Based on the MMOH structure, a hypothesis for an interaction site between MMOH and MMOB was developed in which MMOB was proposed to bind in a "canyon" that exists between the two $\alpha\beta\gamma$ protomers and exposes the protein surface over the buried binuclear iron site. The structural dimensions of MMOB would allow it to bind in this canyon, thereby exerting its effects on the binuclear iron cluster. Unfortunately, neither MMOB nor its complex with MMOH has been successfully crystallized from either of the commonly studied methanotroph species. Consequently, X-ray crystallography could not provide the desired details of the MMOB−MMOH surface interactions.

One distinctive feature of the MMOB solution structure is the presence of both a well-ordered core region (residues 36−126) and disordered N- (residues 1−35) and C-terminal (residues 127−138) regions. Some indication of the manner in which MMOB interacts with MMOH has come from the observation that proteolysis of the N-terminal region of MMOB from *Me. capsulatus* (Bath) readily occurs during purification, leading to a protein that is progressively less able to enhance the rate of catalysis as larger sections of this region are removed (*21, 22*). Proteolysis occurs most readily between M12-G13 and Q29-V30. Mutation of residues within these regions of *Me. capsulatus* (Bath) MMOB to those found in equivalent positions in *M. trichosporium* (OB3b) MMOB made the protein resistant to proteolysis and loss of function. Another indication of the importance of the N-terminal region has been derived from recent mutagenesis studies of *M. trichosporium* OB3b MMOB in which the only two histidines in the protein (H5 and H33) were altered, leading to significant changes in the rate constants for specific steps in the O_2 binding and activation steps in the catalytic cycle via an unknown mechanism (*17*). While it is clear that the N-terminus is important for catalysis, it is not known whether the well-ordered core region also has effects or whether both the N-terminal and the core regions must be present to enhance catalysis.

The structural fold of the core of MMOB does not suggest any obvious areas of MMOH−MMOB interaction. Some insight into the specific areas where this interaction occurs was gained through observation of the perturbation of relaxation characteristics of specific NMR resonances when the oxidized form of MMOH (**MMOH^{ox}**) from *Me. capsulatus* (Bath) was added to its species-specific MMOB (*20*). However, this study was complicated by two aspects of the interaction related to the function of MMOB. First, the complex forms with a dissociation constant in the nanomolar range near neutral pH (*14, 15*). This suggests that the exchange rate may be relatively slow compared with the NMR time scale and also requires that the measurements be made on very low concentrations of proteins so that a population of free MMOB exists in solution as required by the technique. Second, the important interactions of MMOB that lead to the great enhancements in the rate of O_2 binding and activation occur with reduced MMOH (**MMOH^{r}**) rather than **MMOH^{ox}**, and thus a determination of the interactions in the reduced complex is likely to be necessary to understand this role of MMOB in catalysis. Fortunately, both of the problems can be addressed by using NMR spectroscopy to study the interaction of the complex that contains **MMOH^{r}**. This is true because we have previously shown that the affinity between MMOH and MMOB is directly coupled to the redox potential (*15*). The large negative shift of the redox potential of MMOH in the complex requires that the dissociation constant increase by 3−4 orders of magnitude, bringing it into the range where rapid exchange and a significant amount of free MMOB can be expected at NMR-accessible concentrations of the components.

Here two aspects of the MMOB−MMOH interaction are investigated using heteronuclear NMR spectroscopic techniques. First, the complex of MMOB with **MMOH^{r}**, and for comparison **MMOH^{ox}**, is studied to identify areas of interaction on the MMOB surface. Second, a peptide with the same composition as the N-terminal of MMOB is prepared, and its effect on catalysis as well as its interaction with **MMOH^{ox}** and **MMOH^{r}** is investigated.

EXPERIMENTAL PROCEDURES

Materials and Common Methods. Common reagents were the highest grade available and were obtained from either Sigma (St. Louis, MO) or Aldrich Chemicals (Milwaukee, WI). Molecular biological reagents were purchased from either Invitrogen (Carlsbad, CA), Qiagen (Valencia, CA), or New England Biolabs (Beverly, MA). DEAE Sepharose and Sephadex resins were products of Pharmacia (Piscataway, NJ). ^2H_2O (99.9%) was purchased from either Cambridge Isotope Laboratory (Andover, MA) or Isotec, Inc. (Miamisburg, OH). $^{15}NH_4Cl$ (99%) and uniformly labeled ^{13}C-glucose (99%) were obtained from Isotec, Inc. (Miamisburg, OH). Water was purified from deionized water using a Millipore reverse osmosis system. Common methods, including media and agar plate preparation, preparation of freezer permanents and competent cells, plasmid transformations, plasmid minipreparations, restriction enzyme digests,

and other DNA manipulations, were performed as described in Maniatis et al. (*23*) or in the product literature attached to the individual kit or enzyme.

Bacterial Growth and Purification of Recombinant MMOH and MMOB. Bacterial growth of *M. trichosporium* OB3b and the purification of MMOH were as reported previously (*1*, *24*). Recombinant MMOB was prepared from BL21(DE3) or BL21(SI) strains of *E. coli* containing plasmid pBWJ400 in which the position of *mmob* had been optimized with respect to the T7 promoter and ribosome binding site contained in the pT7-7 vector as previously described (*19*).

Preparation of MMOB N-Terminal Deletion Mutant. The mutant *mmob* genes and the initial recombinant *mmob* gene were sequenced by the University of Minnesota Microchemical Facility to confirm the constructs. To construct the Δ2−29 mutant MMOB, the plasmid containing the *mmob* gene (pBWJ400) was treated with the restriction enzymes *Nde*I and *Bst*XI in order to effectively cut the DNA sequence encoding MMOB residues 1−38. The double-stranded oligonucleotide shown below was then constructed that would insert into the cut plasmid to restore residues 1 and 30−38.

5′-TATGCAGGTCGTCCACGAGTCCAACGCC-3′
3′-ACGTCCAGCAGGTGCTCAGGTT-5′

Preparation of MMOB−MMOH NMR Samples. Anaerobic sample handling techniques and the preparation of **MMOH^r** have been previously described by Fox et al. (*1*). In brief, MMOH and methyl viologen (0.1 mol/mol of MMOH) were made anaerobic in 25 mM potassium phosphate buffer, pH 6.8, in a 3 mL conical bottom reaction vial that was Teflon-sealed. The enzyme solution was made anaerobic by flushing the reaction vial with oxygen-free argon gas for 30 min at 4 °C. Anaerobic sodium dithionite was then added stoichiometrically (1 mol of reducing equiv/Fe or 2 mol of reducing equiv/active site) to reduce the MMOH. The reaction was allowed to proceed on ice for about 30 min to ensure that the MMOH was fully reduced. Anaerobic ^{15}N-MMOB and ^2H_2O were added directly to the **MMOH^r**, and the resulting mixture was then transferred into an argon-filled NMR tube that had been subjected to several vacuum/argon cycles. The NMR tube was then sealed by fusing the top. All samples made to study MMOB−MMOH interactions contained 0.2 mM ^{15}N-MMOB, and variable amounts of MMOH in 25 mM potassium phosphate buffer, pH 6.8, 10% D_2O.

Nuclear Magnetic Resonance (NMR) Spectroscopy. MMOB was dissolved in 0.6 mL of ^1H_2O or ^2H_2O containing 25 mM potassium phosphate, pH 6.8. The pH was adjusted by adding microliter increments of 0.1 M NaOH or 0.1 M HCl to the sample. In ^2H_2O, the pH was adjusted for the deuterium isotope effect. The solvent deuterium signal was used as a field-frequency lock. The chemical shifts are quoted in parts per million (ppm) downfield from sodium 4,4-dimethyl-4-silapentanesulfonate (DSS).

All NMR measurements including 2D ^{1}H-^{15}N-HSQC (*25*), 2D NOESY (*26*), and 2D TOCSY (*27*) were done on a Varian Unity Inova 800 MHz spectrometer equipped with an H/C/N triple-resonance probe and *x*/*y*/*z* triple-axis pulse field gradient unit. All spectra were acquired at 25 °C. Carrier frequencies for ^{15}N and ^{1}H were positioned at 116 and 4.7 ppm, respectively. To study MMOB−MMOH interactions, a gradient sensitivity-enchanced version of 2D ^{1}H-^{15}N HSQC was applied with 256 (*t*1) × 1024 (*t*2) complex data points and spectral widths of 2000 Hz in *t*1 (^{15}N) and 9000 Hz in *t*2 (^{1}H) dimensions. Proton homonuclear 2D TOCSY and NOESY were used to investigate structural features of the MMOB N-terminal peptide, as well as peptide−MMOH interactions. A spectral width of 7000 Hz was used in both *t*1 and *t*2 dimensions, with 256 (*t*1) × 2048 (*t*2) complex data points being collected. Raw data were converted and processed by using NMRPipe (*28*) and were analyzed by using NMRDraw. Prior to fast Fourier transformation, raw data were zero-filled to double the size of data points collected, and a 75° shifted squared sine-bell function was multiplied in the time-domain to enhance resolution. In ^{1}H-^{15}N HSQC experiments, a gradient-enhanced version of the pulse sequence was used wherein solvent suppresion was achieved using the gradients. In 2D ^{1}H NMR spectra, the WATERGATE sequence was used for solvent suppression.

HSQC Mapping of the MMOB Binding Interface. HSQC mapping was applied to study the binding interface between MMOB and MMOH. ^{15}N-labeled MMOB was mixed with both oxidized and reduced forms of unlabeled MMOH. Samples containing 0.1 mM MMOB were titrated with 0.01, 0.03, 0.07, and 0.10 mM **MMOH^{ox}** and 0.03, 0.10, 0.13, 0.17, and 0.20 mM **MMOH^r**, and HSQC spectra were acquired at 25 °C for each sample. The intensity of resonances from MMOB in the presence of MMOH was normalized against the intensity of resonances from a 0.1 mM sample of free MMOB.

N-Terminal Peptide of MMOB. To investigate the role of the N-terminus of MMOB, an N-terminal peptide (residues 1−29) with an amidated C-terminus was made using solid-phase peptide synthesis and was HPLC-purified at the University of Minnesota Microchemical Facility. TOCSY and NOESY spectra were acquired in order to characterize the structural features of the peptide and its interaction with MMOH. For the free peptide, NMR spectra were recorded with a sample containing 0.4 mM B peptide in 25 mM potassium phosphate buffer (90:10 H_2O/D_2O), pH 6.8. For B peptide−MMOH interaction studies, 0.2 mM B peptide was titrated with MMOH at B-peptide:MMOH ratios of 1:1, 2:1, 4:1, and 8:1 for the oxidized form and with MMOH at B-peptide:MMOH ratios of 1:1 and 2:1 for the reduced form. ^{1}H TOCSY spectra with a mixing time of 60 ms and NOESY spectra with mixing times of 50, 100, 150, 200, and 250 ms were acquired. "Knock-out" experiments were designed to test the specificity of B peptide binding to MMOH. In this experiment, 0.16 mM MMOB was added to a sample containing 0.2 mM MMOH and 0.2 mM B peptide. If the N terminus of MMOB competed with B peptide for binding, it was expected that B peptide would be displaced or "knocked out" from the MMOH binding site upon addition of MMOB. This was assessed via analysis of TOCSY spectra.

Steady-State Kinetic Measurements. For multiple turnover reactions using nitrobenzene as an assay substrate, reaction rates were monitored at 407 nm for release of the product *p*-nitrophenol ($\epsilon = 15$ mM^{-1} cm^{-1} at pH 7.6, 25 °C) using an Agilent Technologies (Palo Alto, CA) 8453 UV−Vis spectrophotometer. In all cases, the concentrations of reaction components were as follows: 1.0 μM MMOH active sites ($MMOH_{act}$), 1.0 μM MMOR, a variable amount of MMOB, 1.2 mM nitrobenzene, 0.4 mM NADH in 50 mM MOPS,

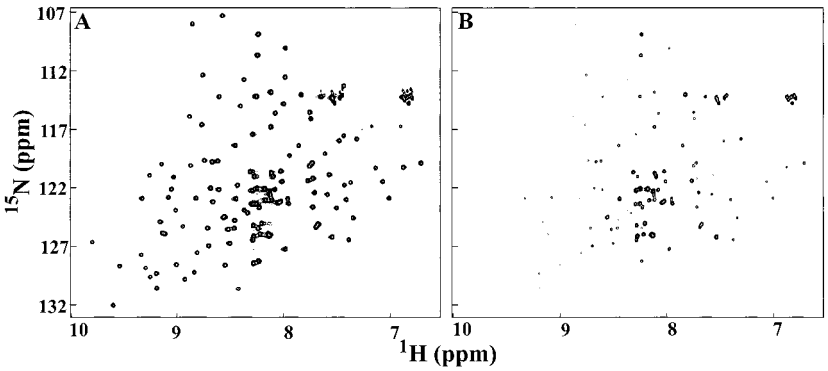

FIGURE 1: ^{1}H-^{15}H HSQC spectra of MMOB. ^{1}H-^{15}N HSQC NMR spectra of ^{15}N-labeled MMOB are shown for free MMOB (panel A) and for MMOB in the presence of **MMOH^{r}** at a 1:1 MMOB:MMOH molar ratio (panel B). Protein concentration was 0.2 mM in 25 mM potassium phosphate at pH 6.8 and 40 °C. Resonance assignments (not indicated here) are given in Chang et al. (*19*).

pH 7.6. The activity for mutated MMOB was normalized to the maximum activity using wild-type MMOB. Concentrations of wild-type MMO components and their respective activities were determined as previously described (*1*, *24*).

Stopped-Flow Absorption Spectroscopy. Transient absorption measurements were all performed using an Applied Photophysics Ltd. SX.18MV stopped-flow spectrometer equipped with the SK.1E extended spectra-kinetic accessory (Leatherhead, United Kingdom). **MMOH^{r}** was prepared as described above and then transferred to one of the stopped-flow drive syringes, being careful not to introduce oxygen. The second syringe contained MMOB and substrate in O_2-saturated 50 mM MOPS, pH 7.0 (unless otherwise indicated). The syringes were allowed to incubate at 4 °C (unless indicated otherwise) for at least 10 min prior to mixing and collecting data. For all experiments, O_2 was added in large excess over MMOH. The intermediates compound P (**P**) and **Q** were monitored by following the reaction at 700 and 430 nm, respectively.

RESULTS

*Interaction between MMOB and **MMOH^{r}***. Upon addition of **MMOH^{r}** to a solution of ^{15}N-labeled MMOB (0.2 mM), ^{1}H-^{15}N HSQC spectra demonstrate that resonances of MMOB are differentially broadened depending on the MMOB:MMOH molar ratio. Figure 1 shows HSQC spectra for free MMOB (panel A) and for MMOB at a 1:1 MMOB:MMOH molar ratio (panel B). Resonance assignments (not indicated here) are given in Chang et al. (*19*). In the presence of this amount of **MMOH^{r}**, HSQC signals from MMOB either are not observed or are significantly reduced in intensity, with the strongest remaining signals being attenuated to about 25% of that observed with free MMOB. Reduction in signal intensity is proportional to the amount of resonance broadening. In reduced MMOH, the ferromagnetically coupled Fe(II)−Fe(II) cluster, having a net spin $S = 4$, could have a considerable effect on the relaxation of MMOB resonances if MMOB were binding close to the iron atoms in MMOH. This effect on relaxation depends on the inverse sixth power of the distance between MMOB and the iron center, as well as on the lifetime of the MMOB−MMOH complex. In oxidized MMOH, the antiferromagnetically coupled Fe(III)−Fe(III) cluster has a net spin $S = 0$ such that it will have no effect on relaxation of MMOB resonances. Because MMOB resonance intensities are overall much larger, i.e., less broadened, in the presence of reduced MMOH than in the presence of oxidized MMOH, resonance broadening in MMOB most probably results from weaker binding to MMOH and not from the spin state of the diiron complex. If MMOB were binding close to the diiron center of reduced-MMOH (within about 20 Å), the effects on NMR relaxation would be substantial and would involve many more resonances than observed here. Since this is not observed, MMOB must be binding MMOH far enough away from the active site to avoid any significant effect on relaxation. It should be noted that the crystal structures of the oxidized and reduced forms of MMOH show that the diiron cluster is buried at least 12 Å from the surface of the protein. Thus, barring a major conformational change in MMOH, the closest approach of the peptide backbone of MMOB to the cluster is likely to be greater than 15 Å independent of where it binds on MMOH.

The presence of differential resonance broadening observed as a function of the MMOB:MMOH molar ratio indicates that molecular interactions are occurring between MMOB and **MMOH^{r}**. To exclude the possibility of nonspecific binding, controls were run in which bovine serum albumin (BSA) was added to the ^{15}N-MMOB solution in equimolar and in 5-fold molar excess. ^{1}H-^{15}N HSQC spectra on ^{15}N-MMOB samples containing BSA were indistinguishable from those run on ^{15}N-MMOB in the absence of BSA, indicating that resonance broadening in the presence of MMOH was the result of specific interactions between MMOB and MMOH. Also, given the fact that MMOB resonances are still observed at the 1:1 MMOB:MMOH ratio, exchange between MMOB and MMOH must be relatively fast on the NMR chemical shift time scale. This, in turn, suggests that binding is relatively weak, consistent with a dissociation constant in the micromolar range as reported previously (*14*, *15*). If binding were strong, one would anticipate the absence or near-absence of resonances at the 1:1 ratio and uniform reduction in resonance intensities at higher ratios. Moreover, the preservation of spectral dispersion indicates that the conformation of MMOB in the MMOH-bound state is relatively unchanged from that of free MMOB (*19*).

This process of HSQC mapping has led to the identification of MMOB resonances that are more broadened in the presence of **MMOH^{r}**. For each residue in MMOB, Figure 2A plots the change in resonance intensity normalized to that from free MMOB (see Experimental Procedures). Data are shown for an MMOB:MMOH molar ratio of 1:1. The

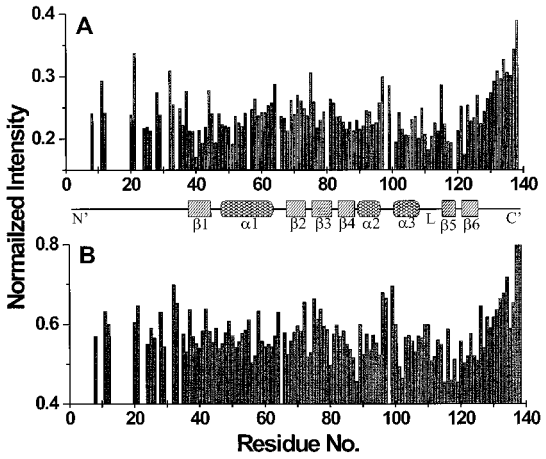

FIGURE 2: Differential broadening of resonances in MMOB. The HSQC resonance intensity from MMOB in the presence of MMOH has been normalized to the HSQC resonance intensity from free MMOB (see Experimental Procedures) and plotted here versus the residue number in MMOB. Data are shown for MMOB in the presence of **MMOH^{r}** (MMOB:MMOH molar ratio of 1:1) (panel A) and in the presence of **MMOH^{ox}** (MMOB:MMOH molar ratio of 3.3:1) (panel B). Secondary structural elements are illustrated in the middle of the plots as coiled lines for α-helices and rectangular boxes as β-strands.

Table 1: The Top 30 Most Broadened Residues of MMOB in the Presence of MMOH

secondary structure	reduced system	oxidized system
N-terminus (1−36)	F24,A26,H33	H33
strand 1 (37−43)	V38,V39,L40,V41, L42,M43	N36,L40
turn 1 (44−46)	D46	D46
helix 1 (47−62)	A50,I51	V56,L57
loop 1 (63−66)		
strand 2 (67−72)	V68	I67
turn 2 (73−74)		A73,G74
strand 3 (75−80)	W77	A80
turn 3 (81−82)		
strand 4(83−87)	I86	I86,D87
turn 4 (88)	A88	A88
helix 2 (89−95)	E90	E90,G92,L95
turn 5 (96−99)		
helix 3 (100−107)	V101,D103,L104,L105	V101,Y102,I106
loop 2 (108−114)	N107,V108,S110,T111, V112, R114	T111,V112
strand 5 (115−118)	L118	A115,T117,L118
turn 6 (119−120)	T120	G119
strand 6 (121−125)	F122	K121,F122,I124, T125
C-terminus (126−138)		E127

most broadened MMOB resonances (top 20%) are associated with residues listed in Table 1 under the column titled "reduced system", and Figure 3 shows the NMR-derived structure of free MMOB (*19*) with these residues highlighted in red. The two structures shown in the column labeled "Reduced system" are related by a 180° rotation in the plane of the page. For the most part, highlighted residues are proximal to each other and identify an area on the surface of MMOB that forms at least part of the interaction interface with **MMOH^{r}**. The structural elements in MMOB that comprise this binding surface arise primarily from β-strand 1 (A37−M43), α-helix 3 (S100−N107), and loop 2 (V108−R114). The orientation of MMOB shown at the top in Figure 3 displays more solvent-exposed surface area than does the backside of that orientation (180° rotation) shown at the bottom of the figure. In fact, most highlighted residues visible in the orientation at the bottom are those that partially protrude through the structure from the orientation of MMOB shown at the top. This is partly a consequence of using backbone NH resonance broadening (as opposed to side-chain resonance broadening) to derive potential binding site residues. In this regard, the orientation shown at the top presents the surface that most probably defines the actual interaction domain with **MMOH^{r}**.

Interaction between MMOB and Oxidized-MMOH. With **MMOH^{ox}**, resonances of MMOB are also differentially broadened, again indicating a molecular interaction between MMOB and **MMOH^{ox}** as known from other experiments (*14*, *15*). However, for **MMOH^{ox}** at the same 1:1 MMOB:MMOH ratio, reduction in signal intensity is significantly greater than the 25% noted earlier with **MMOH^{r}**, dropping to less than 5% of that observed with free MMOB. This difference in the degree of MMOB resonance broadening observed between reduced and oxidized forms of MMOH is consistent with MMOB binding more strongly to **MMOH^{ox}** than to **MMOH^{r}** and provides the rationale for using MMOB:MMOH ratios greater than 1:1 when working with the oxidized state of MMOH in order to more accurately determine differential broadening among MMOB resonances. Although the degree of resonance broadening observed at the 1:1 MMOB:MMOH molar ratio is consistent with the known binding affinity of MMOB for **MMOH^{r}** (micromolar range) (*15*), binding of MMOB to **MMOH^{ox}** has been reported to be in the 10−100 nM range (*14*). At the low end of this range, the system probably would fall into the slow exchange regime on the NMR chemical shift time scale, and one would not expect to observe such broadening effects. Rather one would observe two distinct sets of resonances, one for free MMOB and one for bound MMOB. Given the molecular weight of the MMOB−MMOH complex, resonances from bound MMOB would be highly broadened and would probably not even be observed. The most likely explanation for the observed resonance broadening is that the actual dissociation constant for the binding of MMOB to **MMOH^{ox}** is at the higher limit of that range, i.e., 100 nM.

Figure 2B plots the change in NH resonance intensity for each residue in MMOB, normalized to that from free MMOB, in the presence of **MMOH^{ox}** at a MMOB:MMOH molar ratio of 3.3:1. The most broadened MMOB resonances (top 20%) belong to residues listed in Table 1 under the column titled "oxidized system". As with the "reduced system", these residues are highlighted in red in the NMR-derived structure of free MMOB (Figure 3, left). Orientations of MMOB shown at the top and bottom are the same as those shown at the right for the reduced system. Although in the oxidized system highlighted residues are generally more distributed throughout the structure of MMOB, a good number of them are the same as those observed in the reduced system (L40, D46, I86, A88, E90, V101, T111, V112, L118, and F122), and some of these are part of the surface area identified above as the MMOB binding region to **MMOH^{r}**. However, because other affected residues are scattered throughout the structure of MMOB, the situation with **MMOH^{ox}**, in terms of identifying a binding domain, is not as easy to explain as with **MMOH^{r}**, where residues from one surface patch essentially can account for most

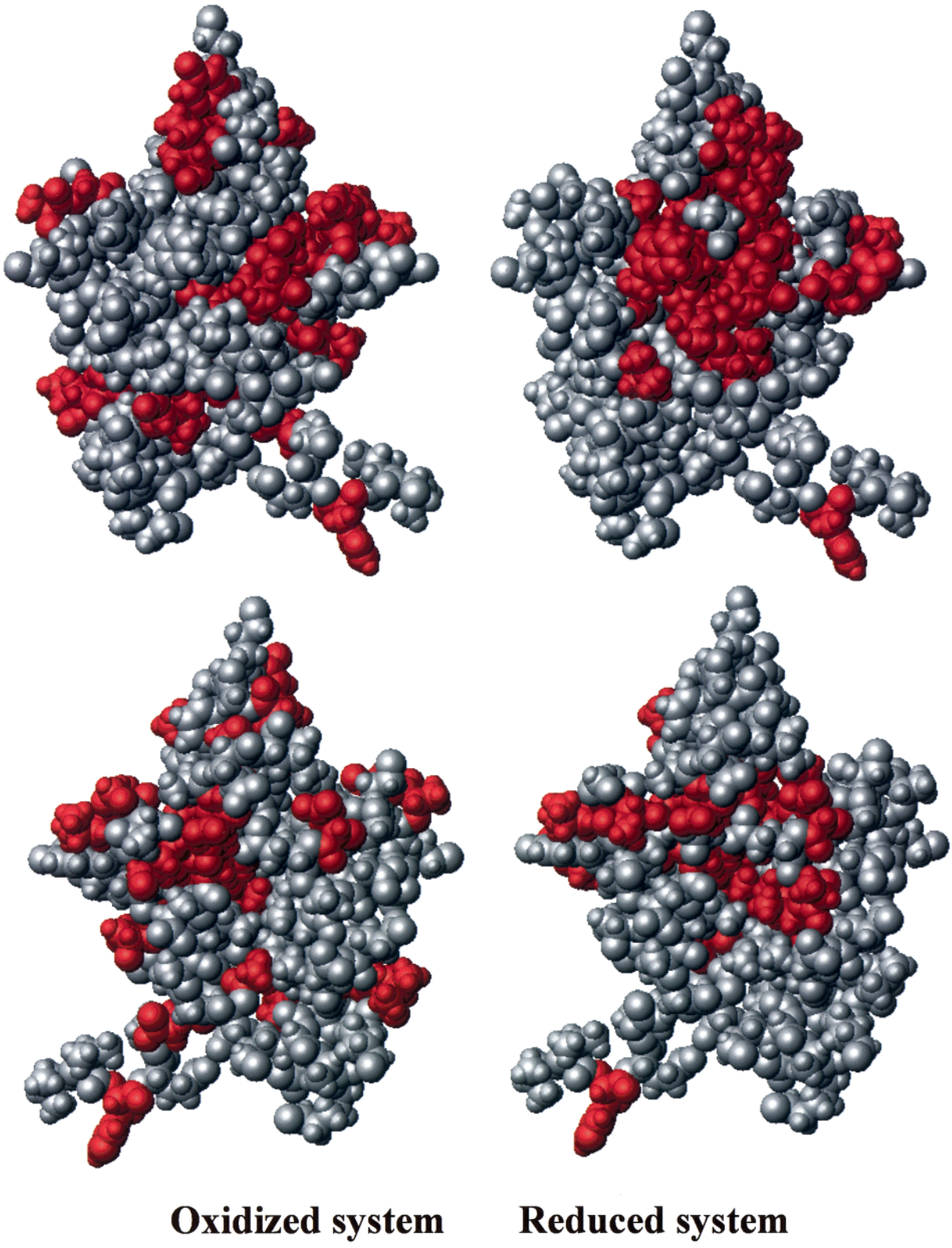

FIGURE 3: NMR-derived structure of MMOB with interacting residues highlighted. NMR-derived structures of MMOB (*19*) are shown. According to Table 1, residues that are highly broadened are highlighted in red (those most broadened) or in yellow. Structures at the left are for MMOB interactions with oxidized-MMOH, and structures at the right are for MMOB interactions with reduced-MMOH. Structures on the bottom have been rotated 180° relative to those at the top of the figure. The structurally nondiscript N-terminus, which is positioned at the bottom of each structure, has been omitted for clarity.

broadened resonances. Three possibilities may help explain this. First, it could be that more of the surface of MMOB is indeed required to interface with **MMOH^{ox}**. Second, because binding of MMOB to **MMOH^{ox}** is stronger than to **MMOH^{r}**, differential resonance broadening may be more difficult to assess. Third, also due to stronger binding, changes in

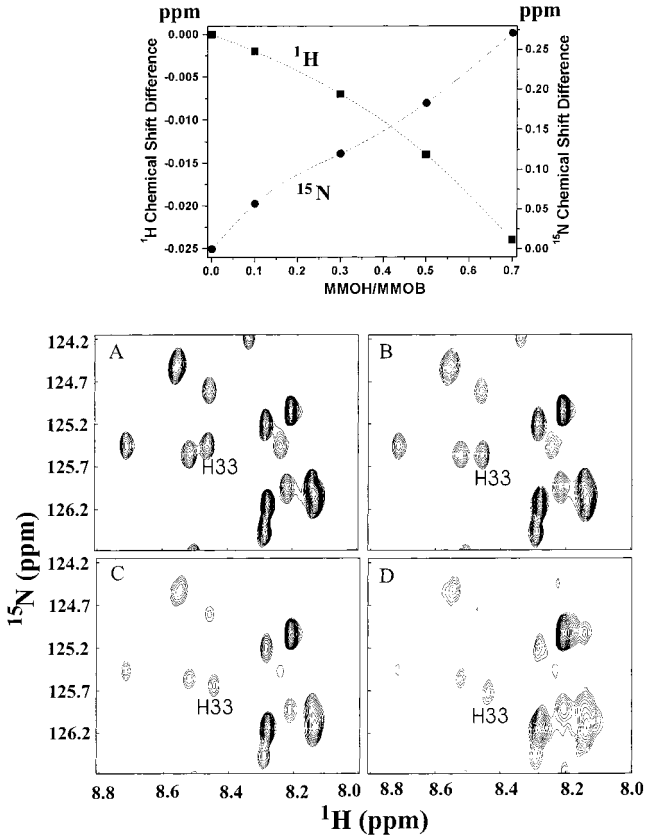

FIGURE 4: HSQC expansions showing H33. Four expansions of HSQC spectra of MMOB acquired in the absence (A) and in the presence of **MMOH^r** [MMOB:MMOH ratios of 3:1 (B), 2:1 (C), and 1:1 (D)]. Notice that in addition to a reduction in intensity, H33 resonances are shifted as the MMOB:MMOH ratio is decreased. This is quantified in the plot at the top of the figure which shows the H33 ^{1}HN and H^{15}N chemical shift differences versus the MMOH:MMOB ratio.

MMOB conformation, internal motions, and/or microscopic binding affinities at the level of individual residues can have greater effects on the relaxation and broadening of resonances in this exchanging system.

MMOH Binding Interface Also Involves the N-Terminus of MMOB. Another group of MMOB residues that forms part of the interaction interface with MMOH, in either reduced or oxidized states, is found within N-terminal residues 1−34. This is supported by two lines of evidence. First, even though both C- and N-termini in free MMOB are highly internally mobile[2] (*19*), several resonances arising from N-terminal residues are considerably more broadened than those from C-terminal residues (Figure 2). Since some resonances from N-terminal residues in free MMOB have not been assigned (*19*), a complete picture is absent. However, within the first 10 residues, resonances from H5 and Y8 have been assigned, and both are significantly broadened relative to C-terminal residues, as well as to many within the structured part of the protein. The second line of evidence comes from the observation that ^{1}H and ^{15}N resonances of H33 are chemically shifted as the MMOB:MMOH ratio is changed. This is exemplified in Figure 4A−D which shows four expansions of HSQC spectra for MMOB in the absence (A) and in the presence of **MMOH^r** [MMOB:MMOH ratios of 3:1 (B), 2:1 (C), and 1:1 (D)]. Notice that in addition to a reduction in intensity, H33 resonances are shifted as the MMOB:MMOH ratio is decreased. This is quantified in the plot at the top of Figure 4 which shows the H33 ^{1}HN and H^{15}N chemical shift differences versus the MMOH:MMOB ratio. These shifts are greater for ^{15}N than for ^{1}H due primarily to the greater ppm range accessible to ^{15}N. No information is available on the other N-terminal histidine, H5, because its assignment is ambiguous. The question then arose as to why only H33 and no other HSQC cross-peaks were observed to shift (only broaden). The most likely explanation is that the more internally mobile N-terminus falls in the appropriate exchange regime and the histidine pK_a is different in the MMOH-bound state. Notice also that the histidine resonances are shifted more upfield as the bound state population is increased. This chemical shift trend in H33 cannot simply be due to variations in the actual solution pH for two reasons: (1) ^{15}N and ^{1}H resonances varied monotonically as a function of the MMOH:MMOB ratio, and (2) no other cross-peaks in these HSQC spectra or in ^{1}H TOCSY spectra (not shown) were shifted. Unfortunately, side-chain resonances of H33, that would have been better indicators for the histidine protonation state, could not be observed in ^{1}H TOCSY spectra. Assuming that chemical shift changes in these ^{15}N-^{1}H backbone resonances do reflect the protonation state of H33, an upfield chemical shift is consistent with the presence of a less protonated state of histidine (*29*). If this were so, the histidine pK_a in the MMOB-bound state would be lower than that in unbound MMOB. One possibility for this is that the MMOB histidine is proximal to carboxylate group(s) on the surface of MMOH.

Interaction of MMOB N-Terminal Peptide with MMOH. Since the question of the role of the MMOB N-terminus is crucial to fully understanding the function of MMOB in its modulating effect on MMOH in the MMO system, additional NMR experiments were performed with a synthetic N-terminal peptide from MMOB (residues 1−29: MSSAHNAYNAGIMQKTGKAFADEFFAEEN, 'B peptide') to assess whether this segment of MMOB by itself can interact with MMOH. The rationale for using a peptide was that binding to MMOH should be weaker than for parent MMOB which would shift the system into a faster chemical shift exchange regime and hopefully improve the ability to observe interactions and transfer NOEs (TRNOEs) with MMOH in both redox states. Initially, sequential ^{1}H assignments for B peptide were made by analysis of homonuclear TOCSY and NOESY spectra. Based on observed sequential NOE connectivities and, in some cases on a process of spin-system elimination, most B peptide resonances could be assigned (Table 2).

The first interaction studies were carried out using **MMOH^r** with B peptide to MMOH ratios of 1:1 and 2:1. B peptide concentration was held constant at 0.2 mM, and changes in B peptide resonance intensities were assessed using TOCSY spectra as exemplified in Figure 5 for free B peptide (panel A) and for B peptide:MMOH ratios of 2:1 (panel B) and 1:1 (panel C). On addition of **MMOH^r** at a 2:1 ratio, most resonances from B peptide were too broad to be observed, while those belonging to C-terminal residues and alanine methyls were least broadened (see Figure 5). At a ratio of 1:1 where a larger population of B peptide is in

[2] S.-L. Chang et al., unpublished data.

Table 2: Proton Resonance Assignments for B Peptide

residue	NH	αH	βH	others
M1				
S2[a]		4.53	3.89, 3.83	
S3[a]		4.41	3.86, 3.8	
A4	8.11	4.15	1.36	
H5				2H 7.91
				4H 7.0
N6		4.59	2.72, 2.66	
A7	8.3	4.19	1.23	
Y8	8.03	4.49	3.1, 2.96	2,6H 7.06
				3,5H 6.77
N9		4.55	2.73, 2.63	
A10	8.2	4.19	1.26	
G11	8.23	3.87		
I12	7.76	4.11	1.83	γ1H 1.38, 1.12
				γ2H 0.84
				δH 0.8
M13	8.29	4.4	2.01, 1.95	γH 2.53, 2.45
Q14	8.26	4.26	2.04, 1.94	γH 2.32
K15	8.35	4.31	1.79, 1.72	γH 1.41, 1.34
				δH 1.61
				εH 2.92
T16	8.08	4.33	4.2	γH 1.16
G17	8.37	3.96, 3.91		
K18	8.09	4.24	1.71, 1.61	γH 1.41, 1.34
				εH 2.92
A19	8.14		1.32	
F20		4.53	3.09, 3.02	
A21	8.3	4.19	1.28	
D22	8.1	4.43	2.63, 2.57	
E23	8.19	4.1	1.79, 1.76	γH 1.94, 2.04
F24	8.09	4.49	2.96, 2.89	2,6H 7.08
				3,5H 7.24
				4H 4.41
F25	7.98	4.48	3.03, 2.92	
A26	8.21	4.19	1.3	
E27	8.24	4.15	1.99, 1.88	γH 2.22
E28	8.48	4.19	1.99, 1.9	γH 2.2
N29	8.37	4.63	2.77, 2.68	

[a] The exact order of the chemical shifts for S2 and S3 is ambiguous.

the bound state, additional resonances become broadened and therefore unobservable, and only those arising from the side chains of S2, S3, the alanines, N29 (weak), and those from backbone groups of I12 (weak), E27, and E28 can still be identified in the TOCSY spectrum. This information is summarized in Figure 6 (top bar graph) which plots relative resonance intensities of groups through the sequence. The height of the bars in the graph is proportional to backbone (hatched) and/or side-chain (shaded) resonance intensity. Not only do these data indicate that B peptide interacts with **MMOH^{r}**, they also suggest that C-terminal (residues A26, E27, E28, N29) and N-terminal (residues S2, S3) segments of B peptide interact least with **MMOH^{r}**, whereas the mid-segment of the peptide interacts more strongly with the enzyme. For this analysis, it was assumed that the appearance of alanine methyl resonances was merely due to their relatively high internal mobility and consequent narrower line widths.

Results with **MMOH^{ox}**, while similar, are somewhat different. In this case, experiments were carried out at B peptide to **MMOH^{ox}** ratios of 8:1, 4:1, 2:1, and 1:1 with the B peptide concentration again being held constant at 0.2 mM. At a ratio of 1:1, the only signals remaining in the TOCSY spectrum were from I12, A26, E27, E28, and N29 and from alanine methyl groups (Figure 7A). At the 2:1 ratio (data not shown), resonances from the C-terminus remained strong; those from the mid-region of B peptide (G11, I12, Q14, A21, E23) increased in intensity, and those from the N-terminus were still too broad to be observed. This information, summarized in Figure 6 (middle bar graph), indicates that, as with the reduced form of MMOH, the C-terminal segment of B peptide (A26, E27, E28, N29) interacts least strongly with **MMOH^{ox}**, whereas the mid-segment and N-terminal segment interact more strongly. Interestingly, S2 and S3 side-chain resonances from B peptide were not observed in the presence of **MMOH^{ox}**, whereas they were observed with **MMOH^{r}** (Figure 6). Also, side-chain signals from E27, E28, and N29, which show up in the presence of **MMOH^{ox}**, are absent in the presence of **MMOH^{r}**. I12 appears in the presence of both reduced and oxidized forms of MMOH. These data indicate that while the interaction of B peptide with reduced and oxidized forms of MMOH is similar, there are some differences which may be related to changes in microscopic binding at the level of individual residues due to slight shifts in the conformation of MMOH that depend on the enzyme's oxidation state.

Even though B peptide has been shown to interact with MMOH, the question of binding specificity arose. In other words, does B peptide bind MMOH at the same site as does parent MMOB? To answer this, a displacement experiment was performed in which MMOB (0.16 mM) was added to a solution containing 0.2 mM B peptide and 0.2 mM MMOH. TOCSY spectra shown in Figure 7 exemplify the results. The TOCSY spectrum in Figure 7A is for 1:1 B peptide: MMOH without added MMOB, and the TOCSY spectrum in Figure 7B is with added MMOB. Upon addition of MMOB, most resonances from the B peptide regain their intensity. Besides C-terminal residues A26, E27, E28, and N29, residues A4, A7, A10, T17, A19, F24, and F25 in the NH- side-chain region and residues S2, S3, and the AMX spin systems including H5, N6, Y8, and N9 show significant increases in intensity. In addition, the H5 ring 2H and 4H resonances are upfield chemically shifted as the MMOH:B peptide ratio is increased, suggesting a decrease in the pK_a of H5 in the MMOH-bound state. The displacement of B peptide by MMOB indicates that B peptide indeed binds specifically and to the same site on MMOH as does MMOB.

The NMR solution structure of free MMOB indicates there is no obvious regular secondary structure at the N-terminus. However, CD data indicate that there is additional helix content in the protein other than that which resulted from the NMR-derived structure (*19*). This implies that there should be additional, transient helix formed at the N-terminal and/or C-terminal segments of MMOB. For free B peptide in solution (Figure 8A), few conformationally informative NOEs are observed in NOESY spectra. However, one NH−NH NOE between E23 and F24 does suggest the presence of a chain reversal at the C-terminal end of the peptide. In contrast, in the presence of **MMOH^{ox}**, B peptide gives a number of transfer NOEs (TRNOEs) that not only supports the idea of B peptide binding to MMOH but also indicates formation of structure in the MMOH-bound state. As illustrated in Figure 8B, TRNOEs include NH−NH NOEs between E23 and F24, F24 and F25, F25 and A26, and F24 and A26, and one $i,i+3$ NOE between E23 αH and A26 NH. These TRNOEs are diagnostic of helix formation from residues E23 to A26. Most other TRNOEs, such as those between Y8 NH/ring and A7 βH_3, are short range, with the

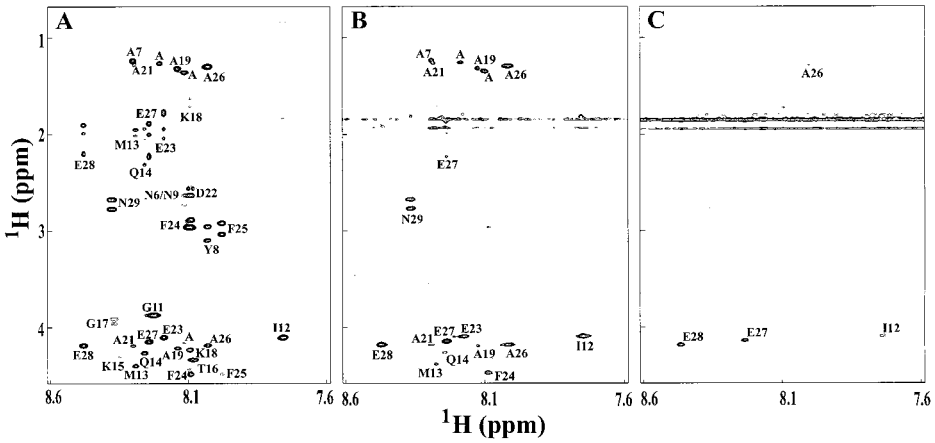

FIGURE 5: TOCSY spectra of B peptide in the absence and presence of **MMOH^r**. TOCSY spectra are shown for free B peptide (A) and for B peptide:**MMOH^r** ratios of 2:1 (B) and 1:1 (C). Assigned cross-peaks have been labeled. On addition of **MMOH^r** at a 2:1 ratio, most resonances from B peptide have disappeared, while those belonging to C-terminal residues and alanine methyls are least broadened.

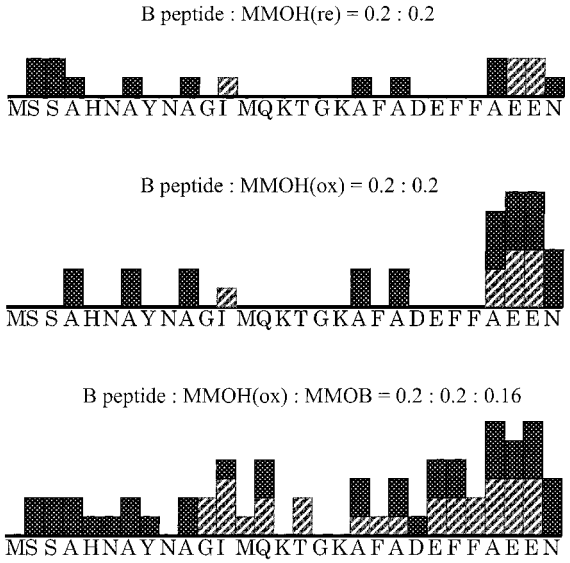

FIGURE 6: Summary of TOCSY resonance broadening in B peptide. Relative resonance intensities of groups through the sequence of B peptide are plotted for B peptide in the presence of 1:1 **MMOH^r** (top bar graph), in the presence of 1:1 **MMOH^{ox}** (middle bar graph), and in the presence of 1:1 **MMOH^r** and 1:0.8 MMOB (bottom bar graph). The height of the bars is proportional to the backbone (hatched) and side-chain (shaded) resonance intensity.

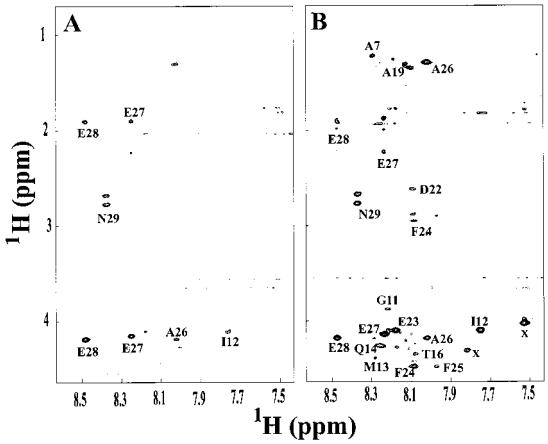

FIGURE 7: TOCSY spectra of B peptide in the absence and presence of **MMOH^{ox}**. TOCSY spectra are shown for B peptide in the presence of 1:1 **MMOH^{ox}** (A) and in the presence of 1:1 **MMOH^{ox}** and 1:0.8 MMOB (B). Assigned cross-peaks have been labeled.

exception of one TRNOE between I12 αH and K15 $\beta/\gamma H_2$ (data not shown) that is also consistent with helix or turn formation within the mid-region of the peptide. In any event, these data suggest that on binding MMOH, the N-terminus of MMOB may adopt a helical conformation.

The N-Terminal Region of MMOB Is Necessary for Its Function. To ascertain whether the flexible N-terminus of MMOB from *M. trichosporium* OB3b is functionally important, a deletion mutant was constructed that lacked residues 2−29 (Δ2−29 MMOB). NMR spectra of the purified mutant protein showed that deletion of residues 2−29 does not significantly affect the structure of the well-folded part of MMOB. However, the mutant was found to be inactive as an enhancer of MMO steady-state activity even when combined with B peptide (see Figure 9, panel A). To determine if this deficiency in increasing MMO turnover rate was accompanied by loss of other MMOB functions, the ability of Δ2−29 MMOB to cause the buildup of intermediates **P** and **Q** in the MMOH catalytic cycle was examined. In stopped-flow single-turnover reactions in which Δ2−29 MMOB in oxygenated buffer was rapidly mixed with **MMOH^r**, it was observed that no **P** (700 nm) or **Q** (430 nm) accumulated in the reaction. This is illustrated in Figure 9 panel B, where the time courses of **Q** formation and decay reactions for wild-type and Δ2−29 MMOB are compared. It should be noted that in both the steady-state and transient kinetic experiments, Δ2−29 MMOB was supplied over a wide concentration range for assurance that loss of ability to act as an effector did not result simply from weaker binding to MMOH. Binding of MMOH and Δ2−29 MMOB was also examined directly using both NMR and fluorescence spectroscopies. Quenching of the intrinsic tryptophan fluorescence of MMOH and Δ2−29 MMOB was observed upon mixing, showing that these two proteins do bind, albeit with less affinity than observed for the wild-type pair (*14*) (data not shown). HSQC mapping using Δ2−29 MMOB has indicated that essentially the same residues as with wild-type MMOB are affected on binding MMOH (data not shown). Finally, it was found that B peptide by itself did not cause enhancement of either steady-state turnover or **P** or **Q** formation.

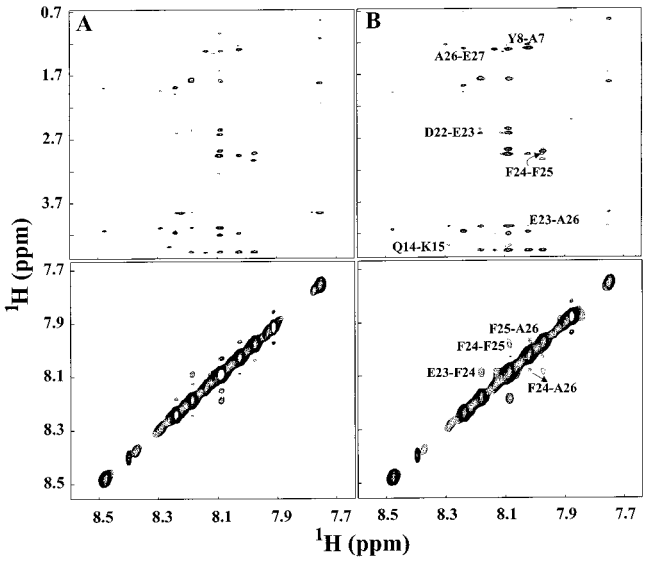

FIGURE 8: Transferred NOEs from B peptide in the presence of **MMOH^{ox}**. NOESY spectra of B peptide are shown for the free peptide (panels A) and for the peptide in the presence of 8:1 **MMOH^{ox}** (panels B). In both sets, panels at the bottom show the NH−NH region of the NOESY spectrum, while panels at the top show the αH/upfield-NH region of the NOESY spectrum. In the presence of **MMOH^{ox}**, B peptide gives a number of transfer NOEs (TRNOEs), some of which are labeled in the figure, that are diagnostic of helix formation.

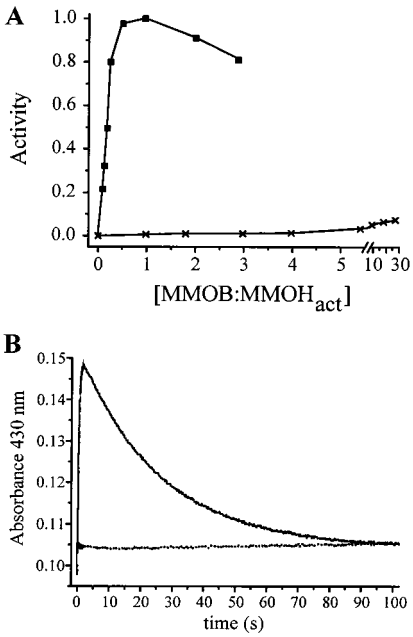

FIGURE 9: Functional assays for Δ2−29 MMOB mutant. Panel A: Δ2−29 MMOB lacks the ability to enhance MMO steady-state activity. The steady-state activity was measured by following the production of *p*-nitrophenol at 404 nm. The assay included 1 mM $MMOH_{act}$, 1 mM MMOR, variable MMOB, 1.2 mM nitrobenzene, 0.4 mM NADH in 50 mM MOPS, pH 7.6, at 25 °C. The activity values were normalized to the maximum value calculated for the wild-type MMOB. *Note:* The addition of up to 50 equiv of the 1−29 peptide did not affect the lack of activity of the Δ2−29 MMOB samples. Panel B: Δ2−29 MMOB cannot enhance Q formation. Q was monitored at 430 nm over 102 s by using stopped-flow absorption spectroscopy (single-wavelength detector). For MMOB (upper trace), the final reaction included 25 μM $MMOH_{act}$, 25 μM MMOB, in 50 mM MOPS, pH 7.0, at 4 °C. For the bottom trace, 100 μM Δ2−29 MMOB and a 200 μM aliquot of the 1−29 peptide were included instead of the full-length MMOB.

DISCUSSION

Results presented here demonstrate that the well-ordered core region of MMOB and also its N-terminal segment both contain residues that form the binding interface with MMOH in both its oxidized and its reduced states. In fact, the N-terminal segment, which is highly internally mobile and conformationally disordered in the unbound state, becomes at least partly helically structured when bound to MMOH. While it is known from previous studies that structural changes occur in MMOH as a result of complex formation with MMOB (*11*, *14*, *15*, *16*, *30*−*32*), this study provides insight into which residues of MMOB facilitate this change. In particular, it provides the first view of the essential interaction between MMOB and **MMOH^r**, the complex in which the novel O_2 gating function of MMOB that initiates catalysis occurs (*12*). In the following sections, these findings are discussed in the context of the structural and mechanistic studies of the components of MMO.

Defining the MMOB−MMOH Binding Interface. The well-ordered region of MMOB is composed of two folding domains: one *βαββ* (A37−G82) and one *βααββ* (A83−T125) (*19*). The first domain is folded such that the α-helix runs almost parallel to the antiparallel *β*-sheet comprising the first three *β*-strands. In domain two, *β*-strand 4 leads into a helix−loop−helix motif with both helices being short two-turn helices, and the segment between helix 3 and *β*-strand 6 is more like a long loop containing short *β*-strand 5. N-terminal residues 1−29 are highly mobile and, therefore, structurally disordered.

The primary interaction surface on MMOB in complex with **MMOH^r** has been highlighted in Figure 3 and defines a reasonably contiguous patch of surface on MMOB that is comprised of residues (see Table 1) primarily from *β*-strand 1 (A37−M43), α-helix 3 (S100−N107), and loop 2 (V108−R114). Aside from this surface patch in the well-ordered region of MMOB, residues from the N-terminus (F24, A26, H33) also particpate in binding to **MMOH^r**, as well as in facilitating the regulatory function of MMOB. In studies with the MMOB N-terminal peptide, it is also evident that other N-terminal residues are involved in binding to MMOH. Moreover, TRNOEs indicate that when bound to MMOH, the N-terminal peptide becomes at least partly helical in structure. The region of the peptide with the clearest evidence for helical structure formation runs from E23 to A26. Note that in HSQC mapping studies with parent MMOB, both F24 and A26, which are part of this helical segment in the peptide, were identified as residues involved in binding. In terms of residue type, most of the "binding" residues listed in Table 1 are hydrophobic (21/30 or 67%). This is consistent with the observation that binding interfaces of protein−protein interactions tend to be highly hydrophobic for relatively strong binding in an aqueous environment. The other types of residues break down as follows: polar uncharged residues, 4 (N107, S110, T111, T120); positively charged residues, 2 (H33, R114); and negatively charged residues, 3 (D46, E90, D103). These may be important in directing the binding orientation when docking to MMOH.

In the **MMOH^{ox}**−MMOB complex, the composition of MMOB residues identified as primarily interacting with **MMOH^{ox}** maintains about the same balance of hydrophobic

(20/30) and polar residues as MMOB in complex with **MMOH^{r}**. In fact, the composition, and in some cases the identity, of polar residues is essentially the same, with 4 polar uncharged residues (N36, T111, T117, T125), 2 positively charged residues (H33, K121), and 4 negatively charged residues (D46, D87, E90, E127). With **MMOH^{ox}**, however, a clear interaction surface on MMOB cannot be readily identified because resonances that are broadened in HSQC spectra of MMOB, in the presence of **MMOH^{ox}**, arise from residues throughout the sequence, and no single surface patch is apparent as is the case with the MMOB−**MMOH^{r}** complex. Nevertheless, a number of residues are the same as those observed in the reduced system (L40, D46, I86, A88, E90, V101, T111, V112, L118, and F122), and, therefore, the same surface area identified as the MMOB binding region to **MMOH^{r}** is also involved in binding to **MMOH^{ox}**. The previous report on the interaction between regulatory protein B and the oxidized state of hydroxylase from *Me. capsulatus* (Bath) (*20*) shows that residues W78 (W77 in MMOB), L96 (L95 in MMOB), G97 (G96 in MMOB), F100 (F99 in MMOB), D108 (N107 in MMOB), G114 (G113 in MMOB), R115 (R114 in MMOB), and Y117 (Y116 in MMOB) are most affected upon binding of MMOB to **MMOH^{ox}**. Even though only L96 is the same in our studies for the oxidized system from *M. trichosporium* OB3b, the regions are essentially nearly the same.

Because only 11 of the 30 most affected interfacial residues are observed in both the reduced and oxidized systems, the orientation of MMOB binding to MMOH is probably different for these 2 oxidation states. This is the first direct evidence that the binding surface is altered by the redox state of MMOH. In the reduced system, the affected residues are located in strand 1, helix 3, and the loop. However, in the oxidized system, although the affected residues are distributed throughout the sequence, to a significant extent, they are concentrated in helix 3, the loop, strand 5, and strand 6. Helix 3 and the loop define at least one interfacial region on MMOB common to binding to both redox states.

At least two explanations may account for apparent differences in MMOB residues that are found to be involved in the MMOB−MMOH binding interface upon reduction of MMOH. First, there may be a genuine difference in the surfaces involved on MMOB, MMOH, or both. In each case, the relative orientation of MMOH and MMOB might change. Alternatively, there might be little shift in orientation, but rather, a significant reorganization of the binding surface through conformational change. Presently, one cannot distinguish between these possibilities. However, the fact that several of the same residues are present in the MMOB binding interface independent of the MMOH oxidation state suggests that the MMOB binding surfaces at least overlap. In addition, because effects of complexation are readily observed in the redox potential of the **MMOH^{ox}** diiron cluster (*15*) as well as in the MCD and EPR spectroscopic characteristics of the reduced MMOH metal center (*1, 16*), it seems likely that MMOB binds in a site near the MMOH active site. This suggests that the MMOB binding sites on MMOH are also at least proximal. The second reason that different MMOB residues may appear to be involved in oxidized and reduced complexes relates to experimental sensitivity. Since binding in the complex is much tighter when MMOH is oxidized (K_d in the nanomolar range), it is likely that either a faster association or a slower dissociation rate constant will result in a longer lifetime of MMOB in the bound state for the oxidized complex. Consequently, since the bound-state MMOB resonances will relax relatively rapidly, the experimental sensitivity will be decreased. Also, there will be a significant decrease in the ability to distinguish intensity differences between resonances belonging to residues that are directly part of the MMOB binding interface from those that are outside of the binding interface. This at least partly explains why the most perturbed residues of MMOB, in the presence of **MMOH^{ox}**, are more distributed throughout its structure. The interaction between MMOB and MMOH is much more readily studied using the reduced system because the dissociation constant falls in the micromolar range, shifting the complex into a more favorable NMR exchange regime. As a result, it is easier to distinguish differences between residues directly involved in binding than those not directly involved.

Although it is unknown where MMOB binds specifically on MMOH, it has been pointed out that association of the symmetrical MMOH $\alpha\beta\gamma$ protomers structurally creates a deep groove or "canyon" over the binuclear iron site (*6*) that is one candidate for the MMOB binding site. This canyon is near the active site of MMOH and has a substantial negatively charged surface potential. Because there is some evidence that the most important MMOH−MMOB interactions are, at least partly, electrostatic in nature[3] (*14*), searching the structural surface of MMOB has led to the identification of a few positively charged areas that may be important for MMOB to bind to MMOH. The most clustered positively charged area in MMOB is near a turn between residues K58 and K63. Current results from HSQC mapping, however, appear to refute this model because the K58−K63 segment is positioned away from the surface on MMOB that interacts with **MMOH^{r}**. Resonances from residues K58−K63 are even less perturbed upon binding MMOH than are most other resonances. Moreover, these data show that negatively charged residues in MMOB are more perturbed than are positively charged residues, suggesting that these negatively charged residues on MMOB interact with positively charged residues on the surface of MMOH. In this regard, the same can be said with MMOB binding to **MMOH^{ox}**.

MMOB N-Terminus Interactions and Function. Another major finding from this study is that the N-terminus of MMOB, which is highly mobile and structurally disordered in the free protein, also interacts directly and specifically with MMOH in both redox states and affects its function. In addition, transfer NOE data indicate that the N-terminal peptide in the bound state possesses elements of helical structure. This information is consistent with that derived from analysis of CD data which suggested that the flexible N-terminus (and/or C-terminus) does form additional helix conformation not differentiable as well-structured helix by NMR (*19*). The primary region of this N-terminal peptide that forms a helix runs between residues E23 and A26. Weaker evidence also suggests helix or at least chain reversal within the I12 to K15 segment. Such lack of clarity may be caused by any number of experimental variables that can

[3] B. J. Wallar and J. D. Lipscomb, unpublished data.

contribute to attenuating the magnitude of TRNOEs; for example, stronger binding with the mid-segment of peptide may lead to differential relaxation terms within the peptide. In fact, residues in the N-terminal peptide that do interact more strongly with MMOH are generally localized within the N-terminal and mid-segment of this peptide. The C-terminal region appears to interact less strongly with MMOH.

A functional role for the N-terminus of MMOB is evidenced by activity studies which indicate that when an N-terminally derived peptide from MMOB or an N-terminal deletion mutant of MMOB that contains only the well-ordered portion of the protein, or a combination of the two, is used, the enhancement of MMO activity characteristic of the native MMOB is not observed. Furthermore, transient kinetic studies show that none of the intermediates of the catalytic cycle form, suggesting that truncation of the N-terminal region slows the reaction at the point of initial O_2 reaction with reduced MMOH. Since the NMR data show that the residues most affected by binding to MMOH are the same for MMOB and the deletion mutant of MMOB, and that the N-terminal peptide apparently occupies the same site on MMOH as the N-terminal region of MMOB, it is likely that the two regions of MMOB must be covalently joined in order to enhance the rate of turnover. Additionally, the data are most easily interpreted under the assumption that interactions from both regions of MMOB are important for catalysis.

Mutations of NMR-Detected Interfacial Residues. Based in part on preliminary results from the current study, several site-specific mutations of MMOB were made (*17*). The changes in function caused by the mutations strongly support the conclusions of the current study in terms of (i) the specific residues identified as being important for interaction in both the core region and the N-terminal segment and (ii) the involvement of both regions of MMOB in catalysis.

One class of MMOB mutants involved changing of one or both N-terminal histidines to alanine. Although these H5A and H33A mutants were found to be nearly fully active in steady-state turnover experiments, transient kinetic studies showed that they altered the rate of O_2 activation leading to **Q** formation. No effects were observed on the rates of steps following **Q** formation. Because product release is rate-limiting in the MMOH catalytic cycle, effects were masked in the steady-state studies. The H33A mutant was found to decrease the rate of **P** formation by at least 50-fold, whereas the H5A mutant decreased the rate of **Q** formation by about 2-fold. The present NMR results suggest that H33 may experience a decrease in pK_a such that it will tend to be more deprotonated in the MMOH complex. This may be related to the fact that the *M. trichosporium* OB3b MMOH−MMOB complex is stabilized by polar and electrostatic interactions[3] which might involve H33. Alternatively, the step in the MMOH catalytic cycle that is slowed by mutation of H33 is that in which a proton is donated to facilitate cleavage of the O−O bond of O_2 during the activation process. Although the immediate donor appears to be very close to the diiron cluster, the proton must be supplied ultimately from solution, and H33 may participate in this process.

A second class of MMOB mutants involved changes in the region of residue T111 which we show here is strongly affected in both the oxidized and reduced MMOH− MMOB complexes. A quadruple mutant, N107G/S109A/S110A/T111A, was prepared which modified the region from hydrophilic to hydrophobic and reduced the size of each of the residues. Remarkably, this mutant accelerated steady-state turnover of large substrates such as furan and nitrobenzene by 2-fold, while leaving the specific activity for methane unchanged. In this case, transient kinetic studies showed that the O_2 activation phase of the catalytic cycle was unaffected, but the substrate reaction with **Q** and product release segments were significantly altered. For large substrates, **Q** reacted 3-fold faster, and the products were released 2-fold faster, accounting for the steady-state results. In contrast, methane was observed to react 7-fold slower with **Q**, but product was released at the usual rate. These results indicate that mutation in this region causes highly specific changes in the interaction of MMOH and MMOB in accord with the NMR results. The results were interpreted in the context of altering the ease of access of large substrates to the active site, which is one way to account for many of the observed effector functions of MMOB. Other mutations within the well-folded region of MMOB near positions that have been shown here to be strongly affected in the **MMOH^r** complex, including residues 26, 101, 104, 105, 114, and 117, have been made, and all lead to nearly complete loss of function. However, transient kinetic studies have yet to be done to determine the specific step(s) of the catalytic cycle that is (are) affected.

REFERENCES

1. Fox, B. G., Froland, W. A., Dege, J. E., and Lipscomb, J. D. (1989) *J. Biol. Chem. 264*, 10023−10033.
2. Woodland, M. P., and Dalton, H. (1984) *J. Biol. Chem. 259*, 53−59.
3. Dalton, H., Wilkins, P. C., and Jiang, Y. (1993) in *Microbial Growth on C1 Compounds* (Murrell, J. C., and Kelly, D. P., Eds.) pp 65−80, Intercept, Ltd., Andover, U.K.
4. Fox, B. G., Surerus, K. K., Münck, E., and Lipscomb, J. D. (1988) *J. Biol. Chem. 263*, 10553−10556.
5. Elango, N., Radhakrishnan, R., Froland, W. A., Wallar, B. J., Earhart, C. A., Lipscomb, J. D., and Ohlendorf, D. H. (1997) *Protein Sci. 6*, 556−568.
6. Rosenzweig, A. C., Frederick, C. A., Lippard, S. J., and Nordlund, P. (1993) *Nature 366*, 537−543.
7. Lee, S.-K., Nesheim, J. C., and Lipscomb, J. D. (1993) *J. Biol. Chem. 268*, 21569−21577.
8. Lee, S.-K., Fox, B. G., Froland, W. A., Lipscomb, J. D., and Münck, E. (1993) *J. Am. Chem. Soc. 115*, 6450−6451.
9. Liu, K. E., Valentine, A. M., Wang, D. L., Huynh, B. H., Edmondson, D. E., Salifoglou, A., and Lippard, S. J. (1995) *J. Am. Chem. Soc. 117*, 10174−10185.
10. Andersson, K. K., Froland, W. A., Lee, S.-K., and Lipscomb, J. D. (1991) *New J. Chem. 15*, 411−415.
11. Froland, W. A., Andersson, K. K., Lee, S.-K., Liu, Y., and Lipscomb, J. D. (1992) *J. Biol. Chem. 267*, 17588−17597.
12. Liu, Y., Nesheim, J. C., Lee, S.-K., and Lipscomb, J. D. (1995) *J. Biol. Chem. 270*, 24662−24665.
13. Liu, Y., Nesheim, J. C., Paulsen, K. E., Stankovich, M. T., and Lipscomb, J. D. (1997) *Biochemistry 36*, 5223−5233.
14. Fox, B. G., Liu, Y., Dege, J. E., and Lipscomb, J. D. (1991) *J. Biol. Chem. 266*, 540−550.
15. Paulsen, K. E., Liu, Y., Fox, B. G., Lipscomb, J. D., Münck, E., and Stankovich, M. T. (1994) *Biochemistry 33*, 713−722.
16. Pulver, S. C., Froland, W. A., Lipscomb, J. D., and Solomon, E. I. (1997) *J. Am. Chem. Soc. 119*, 387−395.
17. Wallar, B. J., and Lipscomb, J. D. (2001) *Biochemistry 40*, 2220−2233.

18. Rosenzweig, A. C., Nordlund, P., Takahara, P. M., Frederick, C. A., and Lippard, S. J. (1995) *Chem. Biol. 2*, 409−418.
19. Chang, S. L., Wallar, B. J., Lipscomb, J. D., and Mayo, K. H. (1999) *Biochemistry 38*, 5799−5812.
20. Walters, K. J., Gassner, G. T., Lippard, S. J., and Wagner, G. (1999) *Proc. Natl. Acad. Sci. U.S.A. 96*, 7877−7882.
21. Lloyd, J. S., Bhambra, A., Murrell, J. C., and Dalton, H. (1997) *Eur. J. Biochem. 248*, 72−79.
22. Brandstetter, H., Whittington, D. A., Lippard, S. J., and Frederick, C. A. (1999) *Chem. Biol. 6*, 441−449.
23. Sambrook, J., Fritsch, E. F., and Maniatis, T. (1989) *Molecular cloning: A laboratory manual*, Cold Spring Harbor Laboratory, Cold Spring Harbor, NY.
24. Fox, B. G., Froland, W. A., Jollie, D. R., and Lipscomb, J. D. (1990) *Methods Enzymol. 188*, 191−202.
25. Kay, L. E., Keifer, P., and Saarinen, T. (1992) *J. Am. Chem. Soc. 114*, 10663−10665.
26. Jeener, J., Meier, B. H., and Ernst, R. R. (1979) *J. Chem. Phys. 71*, 4546−4563.
27. Braunschweiler, L., and Ernst, R. R. (1983) *J. Magn. Reson. 53*, 521−528.
28. Delaglio, F., Grzesiek, S., Vuister, G. W., Zhu, G., Pfeifer, J., and Bax, A. (1995) *J. Biol. NMR 6*, 277−293.
29. Wüthrich, K. (1986) *NMR of Proteins and Nucleic Acids*, Wiley-Interscience, New York.
30. Pulver, S., Froland, W. A., Fox, B. G., Lipscomb, J. D., and Solomon, E. I. (1993) *J. Am. Chem. Soc. 115*, 12409−12422.
31. Liu, K. E., and Lippard, S. J. (1991) *J. Biol. Chem. 266*, 12836−12839.
32. Gallagher, S. C., Callaghan, A. J., Zhao, J., Dalton, H., and Trewhella, J. (1999) *Biochemistry 38*, 6752−6760.

BI0103462